Magnetic Resonance Imaging (MRI) reveals high cardiac ejection fractions in red-footed tortoises (*Chelonoidis carbonarius*)

Catherine J.A. Williams[1,2*], Eva M. Greunz[2], Steffen Ringgaard[3], Kasper Hansen[1,5,6], Mads F. Bertelsen[2] and Tobias Wang[1,4]

[1]Section of Zoophysiology, Department of Bioscience, Aarhus University, 8000 Aarhus C, Denmark
[2]Center for Zoo and Wild Animal Health, Copenhagen Zoo, Roskildevej 38, 2000 Frederiksberg, Denmark
[3]MR Research Center, Department of Clinical Medicine, Aarhus University, Palle Juul-Jensens Blv. 99, 8200 Aarhus N, Denmark
[4]Aarhus Institute of Advanced Sciences, Aarhus University, 8000 Aarhus C, Denmark
[5]Comparative Medicine Lab, Department of Clinical Medicine, Aarhus University, Palle Juul-Jensens Blv. 99, 8200 Aarhus N, Denmark
[6]Department of Forensic Medicine, Aarhus University Hospital, Palle Juul-Jensens Blv. 99, 8200 Aarhus N, Denmark

*corresponding author Catherine.williams@bios.au.dk

Key words: Ejection fraction, stroke volume, MRI, reptile, tortoise.

Summary Statement: Electrocardiogram-gated MRI was used to visualise the cardiac cycle and blood volume movement in red footed tortoises without the need for surgery; determined ejection fraction was over 80%.

Abstract

The ejection fraction of the trabeculated cardiac ventricle of reptiles has not previously been measured. Here we use the gold standard clinical methodology – electrocardiogram (ECG) gated flow magnetic resonance imaging (MRI) – to validate stroke volume measurements and end diastolic ventricular blood volumes. This produces an estimate of ejection fraction in the red footed tortoise *Chelonoidis carbonaria* (n=5) under isoflurane anaesthesia of 88 ± 11%. After elimination of the prevailing right-to-left intraventricular shunt through the action of atropine, the ejection fraction was 96 ± 6%. This methodology opens new avenues for studying the complex hearts of ectotherms, and validating hypotheses on the function of a more highly trabeculated heart than that of endotherms which possess lower ejection fractions.

List of abbreviations

CO cardiac output
f_H heart rate
f_R respiration rate
V_s stroke volume
MRI magnetic resonance imaging
ECG electrocardiogram
EDV end-diastolic volume
ESV end-systolic volume
EF ejection fraction
Et Iso end-tidal isoflurane concentration

Introduction

The heart serves as the permissive pump providing essential convective blood flow to satisfy the metabolic demands of the body. The substrate for cardiac output (CO) is delivered by the rate of venous return to the heart, and CO is the product of heart rate (f_H) and the volume of blood pumped by each cardiac contraction (stroke volume V_s). V_s is the difference between end-diastolic and end-systolic volumes, and animals can therefore increase Vs by elevating end-diastolic volume (EDV) and/or by decreasing end-systolic volume (ESV). Under normal conditions, the ejection fraction (EF) - the proportion of blood ejected in each beat ((EDV-ESV)/EDV) - ranges from 40 to 70% in mammals, meaning that 30-60% of end-diastolic volume resides in the ventricle at the end of each contraction (Hoffmann et al., 2014; Lang et al., 2015). Similar values apply in birds, although considerably less is known about their cardiac function (Harr et al., 2017; Pees et al., 2004). In contrast to these endothermic hearts, EFs of 80-100% have been measured using echocardiography in fish (Coucelo et al., 2000; Franklin and Davie, 1992; Lai et al., 1998; Lai et al., 2004).

The hearts of most ectothermic vertebrates share the common feature of an extensive proportion of spongy myocardium relative to the compact ventricular wall in mammals and birds (Jensen et al., 2013). It has been speculated that the spongy myocardium of the ectothermic hearts permits pressure development and high ejection with minimal myocardial strain (Johansen, 1965; Shiels and White, 2008). However, while low residual ESV and high EFs have been qualitatively reported for reptiles (Burggren and Johansen, 1982; Millard and Johansen, 1974) quantitative measurements are lacking in the literature. This is probably because it is difficult to acquire sufficiently good images of the spongy myocardium to perform quantitative analyses of EF.

Here we take advantage of the clinical gold standard human cardiac imaging technique (ECG gated flow MRI (Hoffmann et al., 2014)) to determine flow in the outflow tract of a tortoise, and we validate these measures of stroke volume by a separate analysis of the dimension of the ventricle in systole and diastole using biplane and volumetric MRI. In combination with postmortem measures of cardiac mass (and hence volume of the ventricular tissue), we derive ejection fraction. To manipulate cardiac output, we applied atropine to abolish the predominant right to left shunt present under isoflurane anaesthesia (Greunz et al., 2018). Our MRI measures confirm a very high EF in this species, with almost 90% of end-diastolic volume being pumped by this reptile heart in each beat.

Methods

Animals

Six female red-footed tortoises (*Chelonoidis carbonaria*, Spix 1824) with a body mass of 3.3 ± 0.8 kg (mean± sd), were used in the study. The tortoises were group-housed at Aarhus University for 6 months in a 6m^2 indoor enclosure (26-28 ˚C, 60-80% humidity, 12:12 light: dark cycle) with hiding places, UV lights (160W UVA+B, Exoterra, Denmark) and heat lamps. There was always access to water and the tortoises were fed daily on mixed vegetables, supplemented by a weekly protein meal. All individuals gained weight, and were deemed healthy based on general clinical examination, white blood cell count, hematocrit and a biochemical profile (Abaxis VetScan VS 2, Scil animal care company GmbH, 68519 Viernheim, Germany). Food was withheld 12 h prior to anesthesia, and procedures were approved by the Danish Experimental Animal Inspectorate (permit # 2015-15-0201-00684).

In a paired cross-over design, randomized for individual order and treatment (using www.random.org), each tortoise was anaesthetized twice, receiving saline or atropine, separated by a minimum of five days. Anaesthesia was induced by inhalation of isoflurane (54 ± 9 min; Vetflurane, VIRBAC, 06516 Carros, France; 4-5 mL of Isoflurane in 50L chamber (Bertelsen, 2019)) to enable topical application of lidocaine (Xylocaine 20 mg/ml AstraZeneca (SE)) to the glottis followed by tracheal intubation with an uncuffed tube (2.3-3.5mm ID silicon endotracheal tube). Maintenance was via a semi-closed circle anesthetic system (Hallowell Small Animal AWS, Pittsfield, MA 01201) with an agent-specific vaporizer (Ventilator Tec 3, Iso Tec, Ohmeda GR Healthcare, Liverpool UK) at four breaths min^{-1} and a tidal volume of 12.5ml kg^{-1}, airway pressure at maximum inflation was 12-15 cm H_2O. Atropine (in 0.9% saline, Sigma Aldrich, Germany, 4 mg/mL) or a matched volume of saline (0.9% sodium chloride Fresnius Kabi, Sweden) were injected into the jugular vein immediately after intubation. MRI Scanning commenced within 43 ± 12 min after injection and lasted 11 to 39 minutes (18 ± 8 min).

End-tidal isoflurane concentration (Et Iso), body temperature, respiration rate (f_R) and heart rate (f_H) were recorded until the animals were placed in the MR-scanner, and again following scanning (equipment: IRMA AX+, Masimo, Sweden Nicolet Elite Doppler, 5 MHz probe, Natus Medical, Inc. Pleasanton, CA 94566 USA). A body temperature of 29-31˚C was maintained using an electric heating pad before scanning (Melissa 631-015; Adexi A/S, Denmark).

MRI safety demands require modification of the ventilation equipment for scanning: longer tubing prefilled with 5% Isoflurane was connected to allow uninterrupted mechanical ventilation and anaesthesia from outside the scan room. The tortoises were mechanically ventilated at a vaporizer setting of 5% isoflurane throughout to prohibit movement within the scanner. f_H monitoring was switched to four limb lead electrocardiogram via non-magnetic clinical attachments, and heating to a digital feedback warm air blower (SAII, Stony Brook, NY 11790, USA). Internal temperature variation between scans of the same individual ranged from 0 to 2.8˚C (1.2 ± 1.4˚ C, mean ± SD).

MRI measurements: flow determination

Flows were measured as described by Greunz et al (2018) in a clinical 1.5T MRI scanner (Philips Healthcare, 1096 BC Amsterdam, The Netherlands), with a head coil as receiver. Anatomical positioning was ascertained via initial localiser scans. Flow measurements orthogonal to the long axis of the heart were derived in the outflow tract using a 7-slice phase contrast flow sequence (Figure 1 A: slice thickness 4 mm, voxel 0.8 x 0.8 mm at 27 frames per cardiac cycle with velocity sensitivity parameter 50 cm/s, supplemental video V2). Flow in the right and left pulmonary arteries, left aorta and right aorta or its branches was processed using software (Siswin, Aarhus, Denmark) in-house developed and analysed by two independent observers blinded to the administration of atropine. Flow was determined in the first slice above the division of the pulmonary trunk into left and right pulmonary arteries, where the circular cross-sectional appearance showed that the slice was orthogonal to the artery long axis. Cardiac long axis views were used to ensure the atropine and saline group slice selection was comparable by confirming the distance from the aortic valves at systole to the slice used for flow measurement (saline distance - 7.62 ± 1.79 mm (mean ± sd), atropine 7.76 ± 1.5 mm). The region of interest was manually corrected over each of the vessels, and flow was calculated in each vessel for each heart phase throughout the cardiac cycle ((Greunz et al., 2018) and **Figure 1 B)**. Inter observer error was 6%: regarded as acceptable to justify

the flow determination method. The mean of the two observers' measurements were used for flow calculations. In one animal it was not possible to obtain good ECG gated images, so data from this animal was excluded.

MRI measurements: volume determination

Views of the heart were acquired via an ECG gated Balanced Steady-State-Free-Precession sequence (slice thickness 2.5 mm and voxel size was 0.8 x 0.8 mm, supplemental video V1). The outer circumference of the ventricle and its length (aortic valve to apex), lateral width and breadth (ventral to dorsal) were marked for each cardiac phase **(Figure 1C)**. Atrial length and area were determined at peak systole and diastole from the slice with largest atrial dimensions, however, the circumferential area throughout the stack was impossible to reliably determine for each atrium, given their complex shape and surrounding structures.

The images corresponding to peak systole and diastole were determined for each ventricle and separately for the atria, and the volume of the ventricle was calculated for an ellipsoid equation (EE)

$v = \frac{4}{3}\pi \bullet 0.5l \bullet 0.5w \bullet 0.5br$, and from volume slicing (VS) summed from the area of the ventricle in each slice x slice thickness. The volume of the atria was estimated as a spheroid based on length and as an ellipsoid based on area in one long axis image and a radius based on atrial length from the same image. Stereological analysis of the ventricles was also attempted using a 5mm random grid, but although end-diastolic, and end-systolic volumes correlated well with values obtained from volumes slicing and ellipse measurements, the variability in the data was greater, and this approach was not taken further.

To further validate our methodology, an excised heart from a *Trachemys scripta* (Thunberg in Schoepff 1792) (0.94 kg male, euthanised with pentobarbital 400 mg kg^{-1} via the subcarapacial sinus) was rinsed and placed in relaxing solution for 2 hrs (NaCl 92mM, KCL 4.7 mM, NaH_2PO_4 1.18mM, $MgCl_2$ 20 mM, $MgSO_4$ 1.17 mM, $NaHCO_3$ 24 mM Glucose 5.5 mM, EGTA 2 mM, EDTA 0.025 mM, pH corrected to 7.4 with NaOH, Sigma-Aldrich Denmark A/S, Copenhagen, Denmark). The ventricle was catheterised via the pulmonary trunk, and the outflow tract and atria were tied off with silk (4/0, Kruuse, Langeskov, Denmark). Known volumes of relaxing solution (0.5,1,1.5,2,3 mL) were injected into the heart and the change in volume was calculated based on the same MRI methods as those used for intact *Chelonoidis carbonaria*. Slice thickness and voxel size were set at half that used in

the tortoises, to give the same number of slices within the smaller ventricle. Stereological analysis of this heart using a 5mm random grid analyzed on all slices with over 400 points within the ventricle analysed revealed a good correspondence of volume determined from the MRI (V_d) with volume added (V_a) to the ventricle, $V_d = 0.9275V_a$, whose $R^2 = 0.9959$.

The mass of the ventricle of the five red-footed tortoises was determined (Sartorius R160P analytical balance) after they were euthanized with IV pentobarbital (400 mg kg^{-1} via the jugular vein) following isoflurane induction. The heart was dissected free of surrounding tissue, placed in heparinised isotonic saline (50 iu mL^{-1} final concentration of heparin 5000 iu mL^{-1} Leo Pharma, Denmark, in 0.9% saline, Fresnius Kabi, Sweden) to aid the dispersion of blood from the chambers, rinsed in further saline, the ventricle dissected at the atrioventricular border, blotted and weighed. Atria were used for determination of smooth muscle in a parallel study and were therefore not weighed.

Volume of the myocardium was initially calculated both for sedentary mammalian densities, and that used in fish studies i.e., 1.05 g cm^{-3} which is also close to the measured value for python ventricular density of 1.068 g cm^{-3} (Franklin and Davie, 1992; Hansen et al., 2012; Vinnakota, 2004) and for the value commonly used in chelonian studies, where density is not known directly 1.00 g cm^{-3} e.g., (Joyce et al., 2014)).

The stroke volume of the heart was calculated by subtracting images of peak systole from peak diastole and compared with the stroke volume produced from the flow measurements in the summed individual vessels. The calculated volumes were used to calculate ejection fraction: $EDV_{(blood)}$ values could be produced by correcting the measured EDV for the presence of trabeculated spongy muscle within the cardiac silhouette by subtracting ventricular cardiomyocyte volume as calculated using the mass of the ventricle and cardiac muscle density of 1.05 mg cm^{-3}. This density assumption and the small measurement error of ventricular mass measurements due to dissection and blotting may account for some measurements of over 100% EF (max 103% in one individual) after atropine treatment.

Ejection fraction was calculated as $(EDV_{(blood)} - ESV_{(blood)})/EDV_{(blood)} * 100$.

Statistical analyses

Paired two tailed t-tests with Welch's correction were used for analysis (De Winter, 2013) in R (R Development Core Team, 2015) using (Mangiafico, 2016). Histograms of difference of paired measurements were inspected to confirm no gross infringement of normality and

homoscedasticity, differences were considered statistically significant at values of $P < 0.05$, effect sizes considered high at > 0.8 (Cohen d), biological relevance is discussed below.

Results and discussion

The cardiac cycle was visualised and flows measured in five intact anaesthetised animals at high temporal resolution (Figure 1A and B and Supplementary video 1 and 2). In accordance with similar flow measurements using surgically placed blood flow probes (Joyce et al., 2018; Overgaard et al., 2002; Shelton and Burggren, 1976; Wang and Hicks, 1996; White and Ross, 1966), the MRI revealed earlier flow in the pulmonary arteries than in the aortae due to the lower afterload (end-diastolic arterial pressure) and the typical prolonged pulmonary flow profile that can be ascribed to the high pulmonary compliance (Figure 1B). Ejection fractions in *Chelonoidis carbonaria* were above 85% (Table 1), which is considerably higher than mammals, but within the range measured by echocardiography in fish (Franklin and Davie, 1992; Lai et al., 2004).

As in mammalian hearts, the cardiomyocytes of spongy ectothermic hearts shorten by approximately 20% during contraction (Shiels and White, 2008). It is therefore believed that the very high EF of the ectothermic vertebrate heart is possible due to the effective nature of many small chambers within the spongy myocardium that can generate pressure and be almost completely emptied (Burggren et al., 2014) without large strain on the myocytes due to the law of Laplace (Johansen, 1965).

Calculated stroke volumes using volume slicing and ellipsoid equation methods corresponded well to measured flow volumes in all individuals, and to injected volumes in the excised *Trachemys* heart (**Figure 2)**. In the excised relaxed heart, the volume contained by the ventricle at zero filling pressure was 0.95-1.5 mL solution kg^{-1} body mass, or 0.86-1.37 mL solution g^{-1} ventricle mass. In the excised heart and *in vivo*, disc-based volumes were significantly higher than those calculated from the ellipse equation, probably partially due to partial volume effects. In this case, biplane MRI provided the best correlation with flow measurements when the intercept was not constrained (R^2 ellipse 0.93, R^2 disc = 0.85) given lower variability, while with intercept constrained to 0, the regression for volumetric measurement lay closer to the line of identity (Figure 2). Previous reports reveal some disparity between biplane and volumetric measurements in axolotls and humans using

echocardiography or MRI with a tendency of obtaining smaller ejection fractions with volumetric measurement in comparison with biplane measurements (Chuang et al., 2000; Gomes et al., 2018). This is also found in this study, where volumetric measures led to slightly, but statistically significantly lower ejection fractions (81 ± 12% and 87 ± 8% after atropine). Although the values of cardiac flow were statistically different from those obtained by the ellipsoid equation, the results show that the biological significance of method choice is low at the cardiac outputs studied here. As shown in Figure 2, the regressions for the volumes produced by the two methods diverge slightly at higher blood flows. Volumetric measurements are more difficult in smaller hearts due to the partial volume effect, and greater resolution scans may be required to specimens smaller than those studied here. Ejection fraction, as expected, remained very high after atropine although end-diastolic volume increased due to the increased rate of venous return from the pulmonary circulation.

Mass adjusted stroke volumes (Table 1) after atropine were similar to the 3.3± 0.3, and 3.07± 0.69 mL kg^{-1} min^{-1} recorded during ventilation or physical activity in recovered *Trachemys scripta* and *Testudo graeca* (Joyce et al., 2018; Krosniunas and Hicks, 2003; Shelton and Burggren, 1976). Stroke volume, however, was lower in our isoflurane anaesthetised tortoises without atropine than the apnoeic or diving conscious chelonians described therein, but similar to pentobarbital anaesthetised *Trachemys* (e.g., Comeau and Hicks, 1994). Heart rates at 30°C are similar to those previously reported for conscious chelonians allowing for Q_{10} effects of body temperature (Johnson et al., 2008; Joyce et al., 2018; Kinney et al., 1977; Kischinovsky et al., 2013; Krosniunas and Hicks, 2003; Shelton and Burggren, 1976; Wang and Hicks, 1996), and lower than pentobarbital anaesthetised or extensively handled animals (Cermakova et al., 2018; Comeau and Hicks, 1994; Crossley et al., 1998; Joyce et al., 2018). The failure of atropine to increase heart rate was unexpected, particularly given the marked effects on the pulmonary circulation that also obey an inhibitory vagal influence (Burggren, 1975), and may be attributed to the isoflurane anaesthesia. It is possible that the direct cardio-depressive effect of isoflurane may have lowered EF (Housmans et al., 2000; Murray et al., 1989). Alternatively, or in addition, isoflurane may have reduced the afterload (through arterial hypotension), which could increase EF compared with that in conscious tortoises given the steep negative relationship between stroke volume and afterload in chelonians (Farrell et al., 1994; Joyce et al., 2016). Measurements were taken at 60 min of anaesthesia, under presumed steady state, but any effect of isoflurane on ejection fraction and cardiac output may have been magnified in the atropine group if atropine, by eliminating the right to

left shunt, led to a greater arterial concentration of isoflurane. Measurements of arterial and venous pressures would enable a disentangling of the effects of atropine, isoflurane and central and peripheral vascular effects of the anaesthetic on ejection fraction.

Atropine caused the expected rise in pulmonary blood flow. The rise in pulmonary venous return increased end-diastolic blood volume and resulted in a doubling of cardiac output (saline vs atropine $p=0.023$) with an elimination of the net right-to-left shunt seen under isoflurane anaesthesia alone as reported in our earlier study (Greunz et al., 2018). Only tentative conclusions can be drawn from our atrial measurements given the great variation in shape observed in the MRI within the studied individuals, but the most concrete measure is of atrial length. In the right atrium, little change was observed in the length and calculated stroke volume of the atria under atropine, however there was a tendency for increased stroke volume of the left atrium after atropine, consistent with increased pulmonary venous return. The measured cardiac outputs under saline and atropine are similar to previous reports in chelonia during apnoea and ventilation, or rest and activity respectively (Joyce et al., 2018; Krosniunas and Hicks, 2003; Shelton and Burggren, 1976). Larger disparities in cardiac output have been reported in some experimental dives in *Trachemys* (Wang and Hicks, 1996; White and Ross, 1966). In conclusion, ECG-gated MRI can provide high resolution data for analysis of the cardiac cycle in complex cardiovascular systems, and here allows the first measurement of high ejection fractions in a reptile.

Supplementary material of video of heart movement under MRI.

Acknowledgements

We gratefully acknowledge the excellent animal care of Heidi Meldgaard Jensen and Claus Wandborg, and the helpful contributions of anonymous reviewers to the final manuscript.

Competing interests – none.

Author contributions

CW, EG, SR, KH, TW and MFB devised the original experiment, CW EG and SR collected the data on *Chelonoidis*, CW and SR analysed flow and collected data on *Trachemys*, CW analysed the remaining data, CW drafted the manuscript. All authors contributed to manuscript preparation and approved its final version.

Funding

CW gratefully acknowledges funding from the Novo Nordisk Foundation, EG is funded by a grant from the Annie and Ottos Johs. Detlefs' Foundation, and TW is funded by the Danish Council for Independent Research, Natural Sciences (FNU).

References

Bertelsen, M. F. (2019). Anaesthesia and analgesia. In *BSAVA Manual of Reptiles*, pp. 200–209. British Small Animal Veterinary Association.

Burggren, W. W. (1975). A quantitative analysis of ventilation tachycardia and its control in two chelonians, Pseudemys scripta and Testudo graeca. *J. Exp. Biol.* **63**, 367–80.

Burggren, W. and Johansen, K. (1982). Ventricular Haemodynamics in the Monitor Lizard Varanus Ex Anthematicus: Pulmonary and Systemic Pressure Separation. *J. Exp. Biol.* **96**, 343–354.

Burggren, W. W., Christoffels, V. M., Crossley, D. A., Enok, S., Farrell, A. P., Hedrick, M. S., Hicks, J. W., Jensen, B., Moorman, A. F. M., Mueller, C. A., et al. (2014). Comparative cardiovascular physiology: Future trends, opportunities and challenges. *Acta Physiol.* **210**, 257–276.

Cermakova, E., Ceplecha, V. and Knotek, Z. (2018). Efficacy of two methods of intranasal administration of anaesthetic drugs in red-eared terrapins (Trachemys scripta elegans). *Vet. Med. (Praha).* **63**, 87–93.

Chuang, M. L., Hibberd, M. G., Salton, C. J., Beaudin, R. A., Riley, M. F., Parker, R. A., Douglas, P. S. and Manning, W. J. (2000). Importance of imaging method over imaging modality in noninvasive determination of left ventricular volumes and ejection fraction: Assessment by two- and three-dimensional echocardiography and magnetic resonance imaging. *J. Am. Coll. Cardiol.* **35**, 477–484.

Comeau, S. G. and Hicks, J. W. (1994). Regulation of central vascular blood flow in the turtle. *Am. J. Physiol. Integr. Comp. Physiol.* **267**, R569–R578.

Coucelo, J., Joaquim, N. and Coucelo, J. (2000). Calculation of volumes and systolic indices of heart ventricle from Halobatrachus didactylus: Echocardiographic noninvasive method. *J. Exp. Zool.* **286**, 585–595.

Crossley, D., Altimiras, J. and Wang, T. (1998). Hypoxia elicits an increase in pulmonary vasculature resistance in anaesthetised turtles (Trachemys scripta). *J. Exp. Biol.* **201**, 3367–3375.

De Winter, J. C. F. (2013). Using the Student's t-Test with Extremely Small Sample Sizes. *Pract. Assessment, Res. Eval.* **18**,.

Farrell, A. P., Franklin, C. E., Arthur, P. G., Thorarensen, H. and Cousins, K. L. (1994). Mechanical Performance of An In-Situ Perfused Heart from the Turtle Chrysemys Scripta During Normoxia and Anoxia at 5-Degrees-C and 15-Degrees-C. *J. Exp. Biol.* **191**, 207–229.

Franklin, C. E. and Davie, P. S. (1992). Dimensional analysis of the ventricle of an in situ perfused trout heart using echocardiography. *J. Exp. Biol.* **166**, 47–60.

Gomes, L., Veld, O., Graaf, D., Sanches, P. G., Roel, C., Graaf, W. De and Strijkers, G. J. (2018). Novel axolotl cardiac function analysis method using magnetic resonance imaging. *PLoS One* **12**, 1–15.

Greunz, E. M., Williams, C. J., Ringgaard, S., Hansen, K., Wang, T. and Bertelsen, M. F. (2018). Elimination of Intracardiac Shunting Provides Stable Gas Anesthesia in Tortoises. *Sci. Rep.* **8**, 17124.

Hansen, K., Pedersen, P. B. M., Pedersen, M. and Wang, T. (2012). Magnetic Resonance Imaging Volumetry for Noninvasive Measures of Phenotypic Flexibility during Digestion in Burmese Pythons. *Physiol. Biochem. Zool.* **86**, 149–158.

Harr, K. E., Rishniw, M., Rupp, T. L., Cacela, D., Dean, K. M., Dorr, B. S., Hanson-Dorr, K. C., Healy, K., Horak, K., Link, J. E., et al. (2017). Dermal exposure to weathered MC252 crude oil results in echocardiographically identifiable systolic myocardial dysfunction in double-crested cormorants (Phalacrocorax auritus). *Ecotoxicol. Environ. Saf.* **146**, 76–82.

Hoffmann, R., Barletta, G., Von Bardeleben, S., Vanoverschelde, J. L., Kasprzak, J., Greis, C. and Becher, H. (2014). Analysis of left ventricular volumes and function: A multicenter comparison of cardiac magnetic resonance imaging, cine ventriculography, and unenhanced and contrast-enhanced two-dimensional and three-dimensional echocardiography. *J. Am. Soc. Echocardiogr.* **27**, 292–301.

Housmans, P. R., Wanek, L. A., Carton, E. G. and Bartunek, A. E. (2000). Effects of Halothane and Isoflurane on the Intracellular Ca2+ Transient in Ferret Cardiac Muscle. *Anesthesiology* **93**, 189–201.

Jensen, B., Wang, T., Christoffels, V. M. and Moorman, A. F. M. (2013). Evolution and development of the building plan of the vertebrate heart. *Biochim. Biophys. Acta - Mol. Cell Res.* **1833**, 783–794.

Johansen, K. (1965). Cardiovascular dynamics in fishes, amphibians and reptiles. *Ann. N. Y. Acad. Sci.* **127**, 414–442.

Johnson, S. M., Kinney, M. E. and Wiegel, L. M. (2008). Inhibitory and excitatory effects of micro-, delta-, and kappa-opioid receptor activation on breathing in awake turtles, Trachemys scripta. *Am. J. Physiol. Regul. Integr. Comp. Physiol.* **295**, R1599-612.

Joyce, W., Gesser, H. and Wang, T. (2014). Purinoceptors exert negative inotropic effects on the

heart in all major groups of reptiles. *Comp. Biochem. Physiol. - A Mol. Integr. Physiol.* **171**, 16–22.

Joyce, W., Axelsson, M., Altimiras, J. and Wang, T. (2016). *In situ* cardiac perfusion reveals interspecific variation of intraventricular flow separation in reptiles. *J. Exp. Biol.* **219**, 2220–2227.

Joyce, W., Williams, C. J. A., Crossley, D. A. and Wang, T. (2018). Venous pressures and cardiac filling in turtles during apnoea and intermittent ventilation. *J. Comp. Physiol. B Biochem. Syst. Environ. Physiol.* **188**, 481–490.

Kinney, J. L., Matsuura, D. T. and White, F. N. (1977). Cardiorespiratory effects of temperature in the turtle, Pseudemys floridana. *Respir. Physiol.* **31**, 309–325.

Kischinovsky, M., Duse, A., Wang, T. and Bertelsen, M. F. (2013). Intramuscular administration of alfaxalone in red-eared sliders (Trachemys scripta elegans)--effects of dose and body temperature. *Vet. Anaesth. Analg.* **40**, 13–20.

Krosniunas, E. H. and Hicks, J. W. (2003). Cardiac Output and Shunt during Voluntary Activity at Different Temperatures in the Turtle, Trachemys scripta. *Physiol. Biochem. Zool.* **76**, 679–694.

Lai, N. C., Graham, J. B., Dalton, N., Shabetai, R. and Bhargava, V. (1998). Echocardiographic and hemodynamic determinations of the ventricular filling pattern in some teleost fishes. *Physiol. Zool.* **71**, 157–167.

Lai, N. C., Dalton, N., Yin, Y., Kwong, C., Rasmussen, R., Holts, D. and Graham, J. B. (2004). A comparative echocardiographic assessment of ventricular function in five species of sharks. **137**, 505–521.

Lang, R. M., Badano, L. P., Mor-Avi, V., Afilalo, J., Armstrong, A., Ernande, L., Flachskampf, F. A., Foster, E., Goldstein, S. A., Kuznetsova, T., et al. (2015). Recommendations for cardiac chamber quantification by echocardiography in adults: An update from the American society of echocardiography and the European association of cardiovascular imaging. *Eur. Heart J. Cardiovasc. Imaging* **16**, 233–271.

Mangiafico, S. S. (2016). *Summary and Analysis of Extension Program Evaluation in R, version 1.15.0.* Rutgers Cooperative Extension New Brunswick, NJ.

Millard, R. W. and Johansen, K. (1974). Ventricular outflow dynamics in the lizard, Varanus niloticus: responses to hypoxia, hypercarbia and diving. *J. Exp. Biol.* **60**, 871–80.

Murray, D. J., Forbes, R. B., Dillman, J. B., Mahoney, L. T. and Dull, D. L. (1989). Haemodynamic effects of atropine during halothane or isoflurane anaesthesia in infants and small children. *Can. J. Anaesth.* **36**, 295–300.

Overgaard, J., Stecyk, J. a W., Farrell, A. P. and Wang, T. (2002). Adrenergic control of the cardiovascular system in the turtle Trachemys scripta. *J. Exp. Biol.* **205**, 3335–3345.

Pees, M., Straub, J. and Krautwald-Junghanns, M.-E. (2004). Echocardiographic examinations of 60 African grey parrot snd 30 other psittacine birds. *Vet. Rec.* **155**, 73–77.

R Development Core Team (2015). R: A language and environment for statistical computing. *R Found. Stat. Comput. Vienna, Austria*.

Shelton, G. and Burggren, W. (1976). Cardiovascular dynamics of the chelonia during apnoea and lung ventilation. *J. Exp. Biol.* **64**, 323–43.

Shiels, H. A. and White, E. (2008). The Frank-Starling mechanism in vertebrate cardiac myocytes. *J. Exp. Biol.* **211**, 2005–2013.

Vinnakota, K. C. (2004). Myocardial density and composition: a basis for calculating intracellular metabolite concentrations. *AJP Hear. Circ. Physiol.* **286**, H1742–H1749.

Wang, T. and Hicks, J. W. (1996). Cardiorespiratory synchrony in turtles. *J. Exp. Biol.* **199**, 1791–1800.

White, F. and Ross, G. (1966). Circulatory changes during experimental diving in the turtle. *Am. J. Physiol.* **211**, 15–18.

Figures

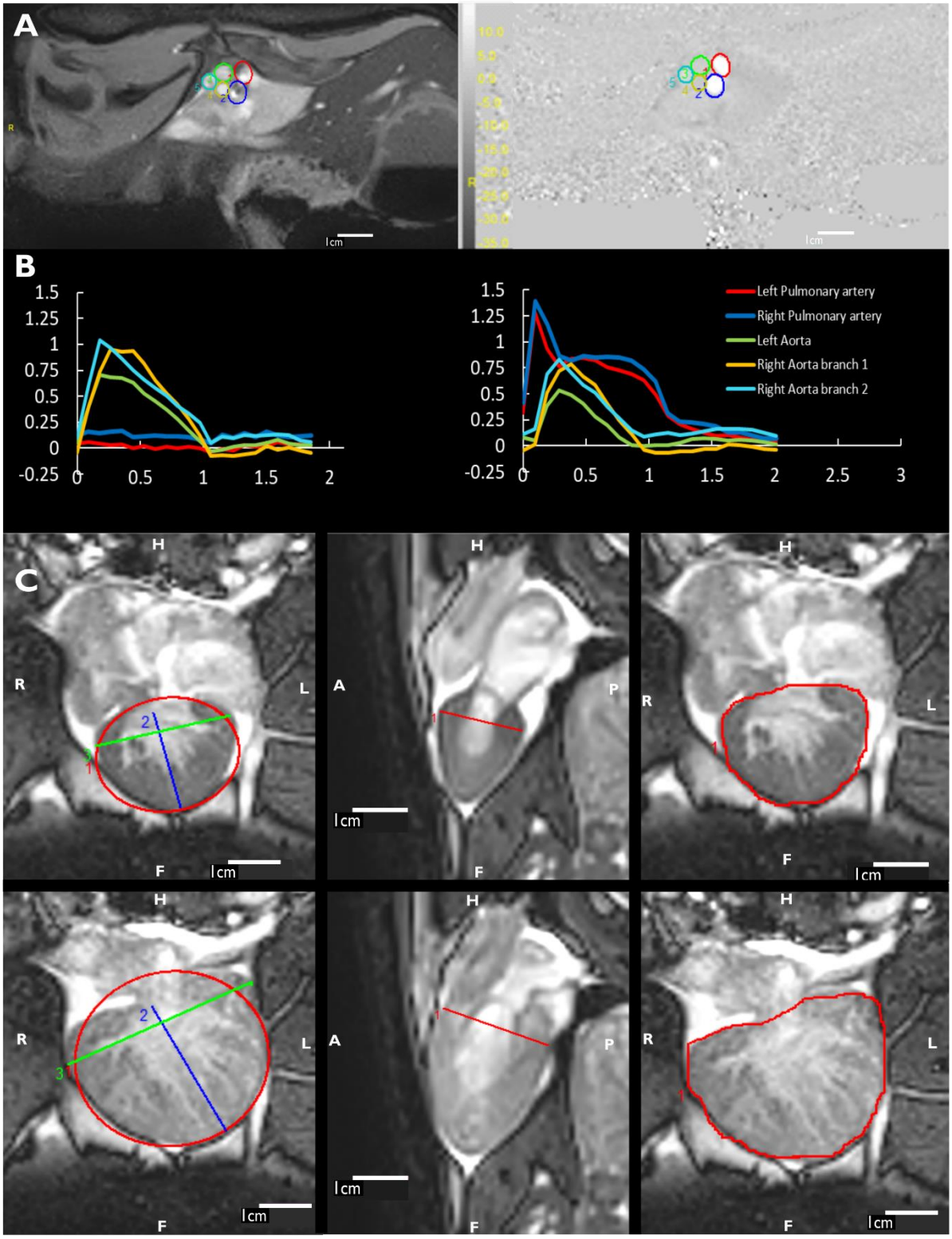

Figure 1 Electrocardiogram (ECG) gated MRI Flow and chamber volume determination for a representative individual *Chelonoidis carbonaria.*

A) Modulus and Velocity images showing regions of interest placed over the major arteries' peri-axial plane, orthogonal to flow, during ventricular contraction. The images are from an animal which received atropine: showing early high velocity flow in the pulmonary arteries (white areas in the velocity image). **B)** Flow (ml s^{-1} kg^{-1}) over time (s) under isoflurane anaesthesia in saline (left) and atropine (right) treatments, produced from images **A**, data replotted as mass specific from (Greunz et al., 2018) and used to validate **C)** Measurements of ventricle volume (ventricular width (green) and length (blue) in coronal plane in the left column and breadth (red) in sagittal plane in the central column, used to calculate volume via the ellipse equation) and ventricle perimeter (coronal plane, used to calculate volume from volume slicing (red)) in the right hand column. Images shown are from peak ventricular systole (upper panel) and diastole (lower panel).

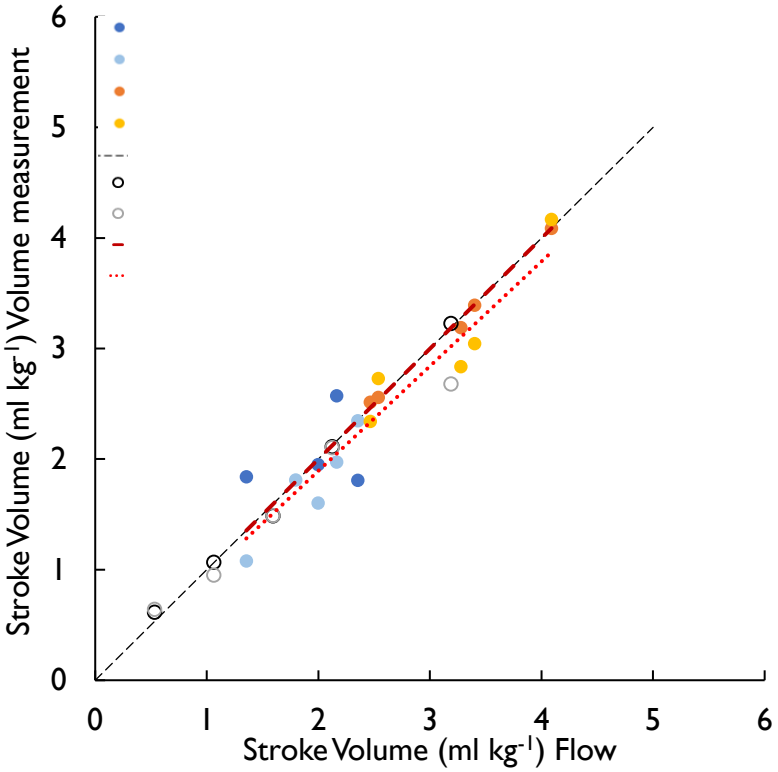

Figure 2 Verification of calculated stroke volumes using flow.

Calculated stroke volumes (mL kg^{-1}) plotted against measured stroke volumes (mL^{-1} kg from outflow tract flow or injected volume) for atropine 1mg kg^{-1} (yellow circle) and saline (blue circle) treated *Chelonoidis carbonaria* (n=5) and an excised heart from *Trachemys scripta* n=1 (open circles). Darker symbols are those where volume was calculated via slice volume (VS) measurements, lighter from the use of the ellipse equation (EE). A line of identity and regression lines for the use of slice volume measurements and the ellipse equation, all with the intercept constrained to 0 are indicated.

Table 1 Cardiac parameters (mean±SD) for isoflurane anaesthetised *Chelonoidis carbonaria* *n=5* treated with Saline or Atropine, calculated using the ellipse method, p values reported for paired two-tailed t.test.

	Saline		Atropine		
	mean	SD	**mean**	SD	p value
Mass ventricle (g)	**4.67**	0.83			
f_H (beats min^{-1})	**30**	5	**30**	2	1
Ventricular parameters relative to body mass					
Ventricular mass (g kg^{-1})	**1.38**	0.18			
SV $_{(flow)}$ (ml kg^{-1})	**1.93**	0.38	**3.15**	0.67	0.001965
EDV blood (ml kg^{-1})	**1.99**	0.48	**3.14**	0.63	0.002256
ESV blood (ml kg^{-1})	**0.23**	0.20	**0.12**	0.19	0.220571
SV $_{(calculated)}$ (ml kg^{-1})	**1.76**	0.47	**3.02**	0.69	0.005233
CO (f_H *SV$_{(Flow)}$) (ml kg^{-1} min^{-1})	**56.99**	9.28	**94.89**	22.33	0.022597
Ejection Fraction %	**88.37**	10.61	**96.05**	6.08	0.137617
Atrial parameters relative to body mass					
Right atrial volume (diastole, ml kg^{-1})	**1.50**	0.80	**2.59**	1.06	
Right atrial volume (systole, ml kg^{-1})	**0.41**	0.30	**0.79**	0.44	
Right atrial stroke volume (ml kg^{-1})	**1.09**	0.64	**1.80**	0.72	
Left atrial volume (diastole, ml kg^{-1})	**0.63**	0.29	**1.36**	0.92	
Left atrial volume (systole, ml kg^{-1})	**0.24**	0.13	**0.31**	0.13	
Left atrial stroke volume (ml kg^{-1})	**0.39**	0.22	**1.04**	0.81	

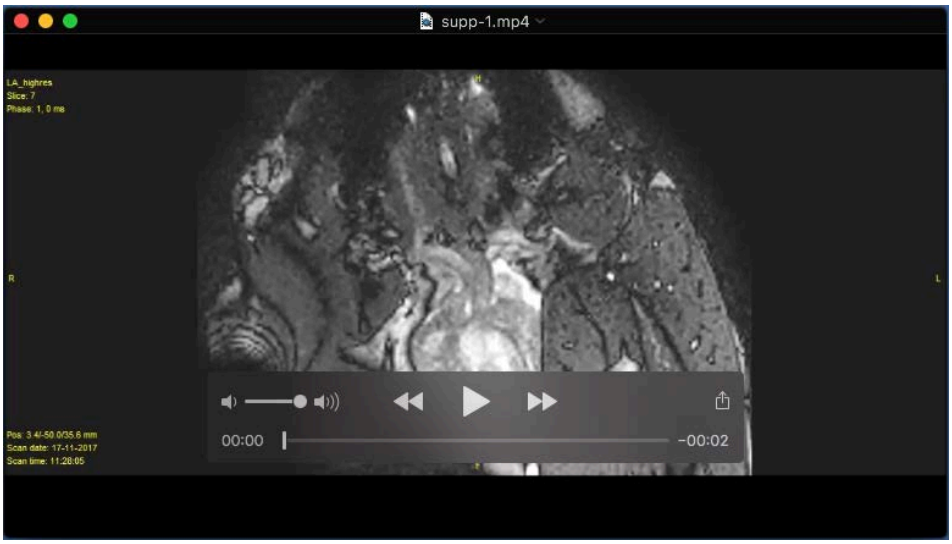

Movie 1. Coronal long axis view.

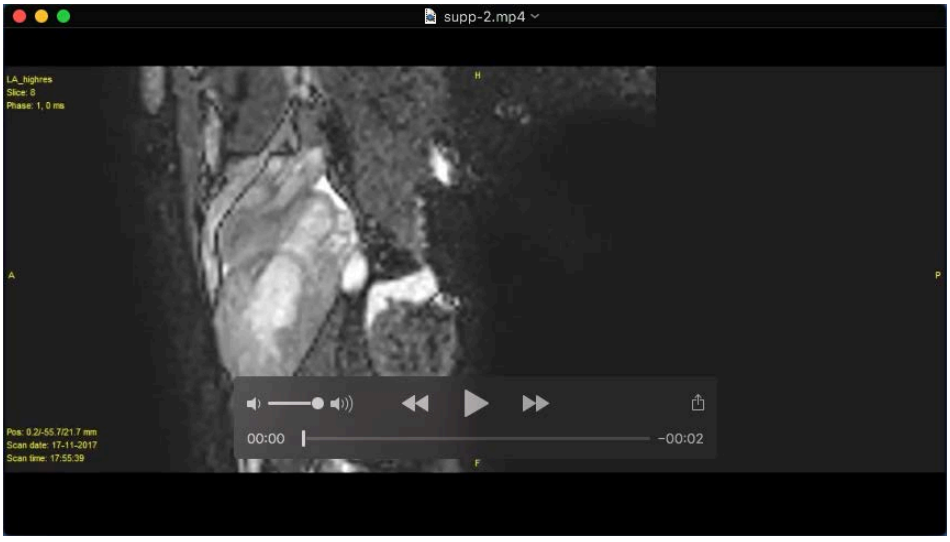

Movie 2. Sagittal long axis view.

Journal of Experimental Biology • Supplementary information